Optics Letters

Verification of transverse translation diverse phase retrieval for concave optical metrology

Aaron M. Michalko* and James R. Fienup

The Institute of Optics, University of Rochester, Rochester, New York 14627, USA
**Corresponding author: aaron.michalko@rochester.edu*

Received 27 July 2018; accepted 29 August 2018; posted 5 September 2018 (Doc. ID 340866); published 1 October 2018

The surface figure error of a concave spherical mirror was measured using transverse translation diverse phase retrieval (TTDPR), an image-based wavefront sensing technique. Good reproducibility of the surface measurement is demonstrated. Additionally, the TTDPR measurement of the surface, with certain alignment terms removed, is shown to agree with interferometric measurements to 0.0060 waves root mean square.

OCIS codes: (100.5070) Phase retrieval; (120.3940) Metrology; (120.6650) Surface measurements, figure.

https://doi.org/10.1364/OL.43.004827

Transverse translation diverse phase retrieval (TTDPR) [1–6] is a robust, ptychographic method of phase retrieval [7–10] that has applications in image reconstruction [11], wavefront sensing [2,4], and as-built hardware characterization [5,12]. In general, TTDPR is used to reconstruct an optical field of interest, $g(x,y)$, based on the measured intensity of light propagated from $g(x,y)$ to a plane near its focus. We can express the field of interest in the form

$$g(x,y) = |g(x,y)| \exp\left[\frac{i2\pi}{\lambda} W(x,y)\right], \tag{1}$$

where $W(x,y)$ is the optical path error, sometimes termed the wavefront aberration function, and λ is the wavelength of illumination. Often, for optical systems testing, $W(x,y)$ is the desired measurand of TTDPR, because the wavefront aberration of a system correlates with parameters such as misalignment and optical defects. Due to its robustness and high wavefront-sensing accuracy, TTDPR is a viable method for not only optical systems testing, but also optical surface metrology [6]. For surface metrology, $W(x,y)$ can be characterized using light reflected off the surface of interest, and used to calculate surface sag departure from nominal. Although TTDPR configurations for measuring convex optics can be conceived [13], TTDPR is particularly attractive for concave surface measurement, because the optical properties of a concave surface in reflection facilitate a simple experimental arrangement. Concave surface measurements with TTDPR may require only an optical source, a translating subaperture mask, and an array detector as described in [6]. Due to these relatively simple hardware requirements, TTDPR systems may be several times less expensive than interferometers for optical shop testing, in particular stitching interferometers, which require complicated optical and motion control components [14]. Furthermore, unlike interferometry, a TTDPR system will not suffer from retrace errors. As a result, TTDPR may be suitable to accurately measure surfaces with rather large aspheric or freeform departures without requiring a null optic [15]. Finally, a TTDPR configuration is flexible and scalable to facilitate a range of test part sizes. TTDPR may be used to make full-aperture measurements of much larger optics than focus-diverse phase retrieval [16], which is limited to high-$F/\#$ measurements and consequently smaller aperture optics.

In the context of optical shop testing, TTDPR has been previously demonstrated as a method for measuring transmitted wavefront error, e.g., of a single refractive optical element, as shown in [3]. In order to broaden its application range, we have extended the capabilities of TTDPR to accommodate optical surface testing. In this Letter, we report on the measurement of a concave optical surface using reflective measurement geometry. Furthermore, we for the first time, to the best of our knowledge, quantitatively compare TTDPR measurements with independent reference measurements of the same surface. Although the wavefront measurements reported in [3] showed a high degree of repeatability, they were not compared against an independent reference measurement, which is necessary to demonstrate the accuracy of the technique.

In TTDPR for surface metrology, a known illumination pattern, $A(x,y)$, is first projected onto the surface of interest. The illumination pattern is translated over the surface, creating a resulting reflected field that we can model as

$$g'_k(x,y) = A(x - x_k, y - y_k) g(x,y) \tag{2}$$

for each translation (x_k, y_k). This field is then propagated to a distant plane, often near the focus of the field of interest, and the intensity pattern

$$I_k(u,v) \propto |\boldsymbol{P}_{x\to u, y\to v}[g'_k(x,y)]|^2 \tag{3}$$

is recorded on an array detector, where $\boldsymbol{P}[\cdot]$ is a Fourier transform or another appropriate propagator. We ensure that each intensity pattern is adequately sampled by the detector using a calculated sampling parameter, Q, given by

$$Q = \frac{\lambda F/\#}{d_u}, \tag{4}$$

where $F/\#$ is the system working f-number calculated using the width of $A(x,y)$ divided by the propagation distance to the detector, and d_u is detector pixel pitch [3]. Q is a measure of sampling density, with $Q = 2$ indicating Nyquist sampling of intensities. The illumination is translated to as many overlapping positions as necessary to cover the surface of interest, with intensities recorded on an array detector for each position. By translating the illumination pattern, we are able to effectively measure a much larger optical surface than would be possible using focus-diverse phase retrieval.

A nonlinear optimization algorithm is then used to estimate $g(x,y)$ using the ensemble of measured intensities by minimizing a data-consistency metric, E, which compares intensities of digitally propagated fields with measured intensities. We used a mean-squared error of intensities metric, given by

$$E = \frac{\sum_k \sum_{u,v} w_k(u,v)\{D_k(u,v) - [\alpha_k I_k(u,v) + \beta_k]\}^2}{\sum_k \sum_{u,v} w_k(u,v) D_k(u,v)^2}, \tag{5}$$

where $D_k(u,v)$ is the kth measured intensity distribution in the detector plane, $w_k(u,v)$ is a bad-pixel mask, and α and β are parameters that can be calculated using Eq. (C3) in [5] to make E invariant to detector gain and bias. E was minimized using the L-BFGS algorithm [17], and analytic derivatives of E with respect to various test parameters were calculated according the equations in [5,18].

We explored the performance of TTDPR for surface metrology through the laboratory measurement of a 75 mm diameter, 1000 mm radius of curvature concave spherical mirror using the experimental configuration shown in Fig. 1. Parts of this experiment were discussed in [19,20]. A 5 mW red HeNe laser, $\lambda = 632.8$ nm, was used as the source in this system. Power was attenuated using a neutral density filter wheel, and the beam was steered through a spatial filter composed of a 20×, 0.40 numerical aperture (NA) microscope objective lens and pinhole to create an apparent point source. A 6.35 mm diameter circular mask was mounted to motorized linear stages with 50 mm range and positioned downstream from the pinhole to realize a translating subaperture. The mirror under test was positioned at a distance of 1000 mm away from the spatial filter source, which is the radius of curvature of the test surface. A fold mirror was used to compact the system and ensure that the reflected beam would not be clipped by the moving subaperture. This initial geometry is analogous to the interferometric null configuration for spherical surface testing, with a point source positioned at the center of curvature of a surface under test. However, instead of measuring the interference of the reflected field with a reference beam, we are directly measuring the reflected light from the mirror near its focus. The test mirror was additionally rotated approximately 2°, so that the reflected field was not blocked by the fold mirror. This rotation simplified the system configuration, at the cost of inducing some third-order astigmatism into the measurement. A Qimaging Retiga 2000R scientific CCD camera with 7.4 μm pixels was used to record each intensity pattern. The camera was positioned at a plane that induced approximately 3 waves peak-to-valley defocus into the global wavefront, because the addition of defocus can improve the performance of phase retrieval when other aberrations are small [8,9,21]. Assuming the camera was located 1000 mm from the mirror, the effective $F/\#$ of the unobstructed system would be 13.33, yielding $Q = 1.14$, according to Eq. (4), which is undersampled for intensities. The subaperture mask projected a circular pattern on the mirror with an approximate diameter of 26 mm. With the subaperture mask in place, the effective $F/\#$ was increased to 38.5, yielding $Q = 3.3$, making each intensity pattern adequately sampled by the detector.

First, a set of measurements was taken to investigate TTDPR reproducibility. Surface error was reconstructed using datasets from two subaperture scan patterns, which are shown in Fig. 2. All other experimental parameters were kept constant. For a given surface measurement, the subaperture was translated to 46 unique positions, giving 46 data intensities. Camera exposure was automatically adjusted for each measured intensity pattern in order to fill most of the dynamic range of the detector. These data were then used in a phase retrieval algorithm to reconstruct the full complex field (amplitude and phase) at the mirror plane. The wavefront was modeled using a superposition of 500 standard Zernike polynomials [15]. The translating subaperture illumination pattern was simulated in the computer as a uniform circular amplitude, although the true illumination had some edge diffraction from the clipping subaperture. Subaperture position, subaperture size, and Q, although assumed well known, were also refined [3] in the later stages of optimization.

Figure 3 shows measurements of wavefront aberration and surface topography error. To obtain these data, piston, tip-tilt, and power (PTP) were first removed from the reconstructed wavefronts using a least-squares fit over a 67.5 mm diameter circular region, 90% the full aperture of the mirror.

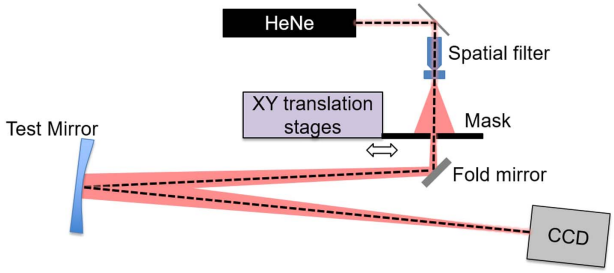

Fig. 1. Experimental configuration for concave TTDPR measurement (not to scale). Computer-controlled stages translate a clipping mask left to right and in and out of the page to create a translating subaperture illumination pattern.

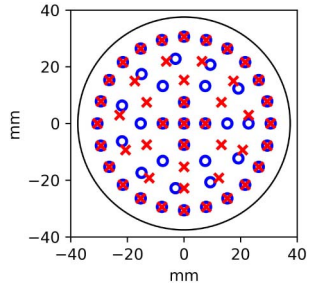

Fig. 2. Scan patterns (centers) used for TTDPR measurements. Blue ○: scan pattern 1. Red ×: scan pattern 2. Black circular boundary: edge of test mirror.

The residual measured wavefront was dominated by astigmatism due to mirror tilt, as shown in Figs. 3(a) and 3(b). Using lens design software, we found the amount of measured astigmatism to be consistent with a tilt angle of approx. 2.08°. This value is within the positioning uncertainty of the manual rotation stage used to align the mirror. In this experiment, we did not have a way to externally verify the mirror tilt angle, so astigmatism was removed from calculations of mirror surface error. In the future, an experiment may be designed so that mirror tilt can be directly measured by using reference flats and an autocollimator. Astigmatism may also be calibrated out of future measurement by measuring the mirror at multiple clocking angles and analyzing the rotationally variant and invariant components [22].

Surface error was calculated using the relationship

$$\Delta z = -\frac{W}{2\cos(2°)} \approx -\frac{W}{2}, \tag{6}$$

where the minus sign corrects the sign conversion from optical phase to surface sag, the cosine factor approximates the effect of mirror tilt, and the factor of two accounts for the double pass. Figs. 3(c) and 3(d) show surface error, calculated using Eq. (6) with PTP and astigmatism removed. These results from the two

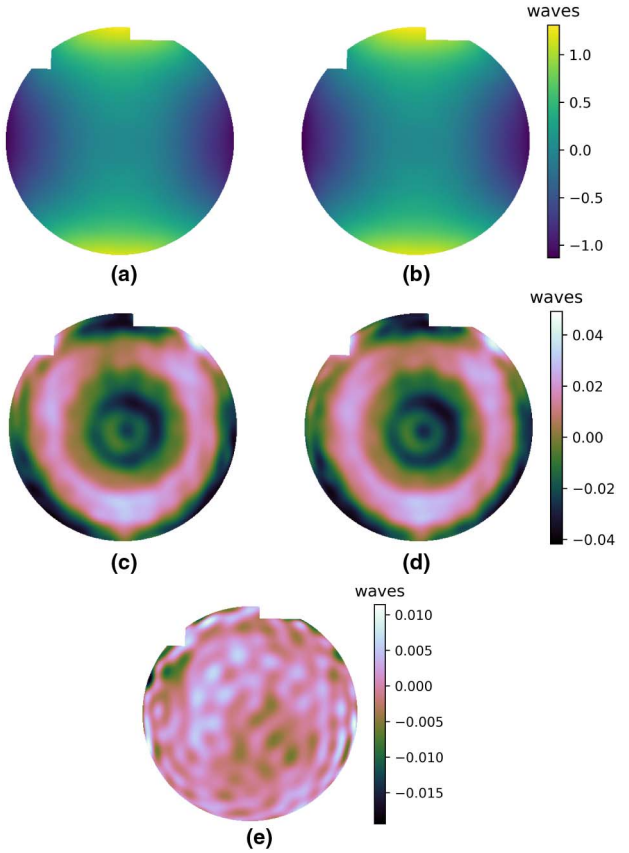

Fig. 3. TTDPR reconstruction over a 67.5 mm diameter area of interest. (a) Retrieved wavefront from scan pattern 1 with piston, tip-tilt, and power (PTP) removed. (b) Retrieved wavefront from scan pattern 2 with PTP removed. (c) Surface error from scan pattern 1, calculated with PTP and astigmatism removed. (d) Surface error from scan pattern 2, with PTP and astigmatism removed. (e) Difference between (c) and (d). Two "notch" fiducials were used to establish a local coordinate system on the surface for comparison.

different subaperture scan patterns agree with one another to 0.0027 waves, or 1.7 nm root mean square (RMS).

Next, reference measurements of the mirror surface were taken using both a ZYGO Verifire and a ZYGO Dynafiz interferometer for comparison with TTDPR. The TTDPR data used for comparison correspond to scan pattern 2. Both sets of interferometric measurements were taken using phase shifting in a standard null configuration with an $F/3.5$ transmission sphere. To allow for quantitative data comparison, fiducials were used to register interferometric data with TTDPR reconstructions to correct for differences in camera resolution, mirror offset, and clocking. To register the data, the overlap between the TTDPR-reconstructed mirror aperture and a bilinear-interpolated interferometer-supplied data mask was optimized to estimate the relative subpixel shift, scale, and clocking of the interferometer measurements relative to TTDPR [5]. Two "notch" fiducials, placed in the aperture of the mirror under test, defined a local 2D coordinate system on the surface and facilitated precise registration of these data masks. Only the mirror aperture, not the measured surface error, was used in the registration procedure to avoid potentially over-fitting the datasets. After registration, the optimized bilinear interpolation parameters were applied to the interferometer-supplied phase data to obtain a phase measurement with the same resolution, clocking, and offset as the TTDPR reconstruction. These phase images were cropped to 90% the full mirror aperture, and PTP was removed. Because astigmatism had been removed from the TTDPR data, it was removed from the interferometric data as well for comparison. The magnitude of removed astigmatism was small, approx. 0.0047λ, or 3.0 nm, RMS. Additionally, because TTDPR used a Zernike superposition to model the measured surface, the TTDPR reconstruction had reduced high-frequency content compared to the pixel-by-pixel variations allowed by the detectors in an interferometer. Although a point-by-point phase map may be used in phase retrieval, it was not used for these reconstructions. As a result, TTDPR and interferometric data were compared with two types of filtering applied. First, they were compared with only low-order aberration terms (PTP plus astigmatism) removed from the interferometric data, i.e., high-pass filtering. Next, they were compared after projecting the interferometer data over the same Zernike basis set used for TTDPR, which would filter out any frequencies outside the range of the TTDPR measurements, i.e., band-pass filtering. Figure 4 shows registered interferometer measurements and computed differences with a TTDPR measurement from each interferometer, with both high-pass and band-pass filtering applied to the interferometer data. Regions of known data dropout in the interferograms were not included in these calculations. Next, the same registration and filtering operations described previously were used to compare results between the two interferometers. Figure 5 shows computed differences between the interferometer measurements with both types of filtering applied. The RMS differences among the various measurements were calculated, and are summarized in Table 1. The best agreements were observed over band-passed interferometer data, where TTDPR agreed to interferometric data to $<0.0068\lambda$, or 4.3 nm, RMS. However, as seen in Table 1, the agreement of TTDPR to either interferometer was comparable to the agreement between the two interferometers for both types of filtering.

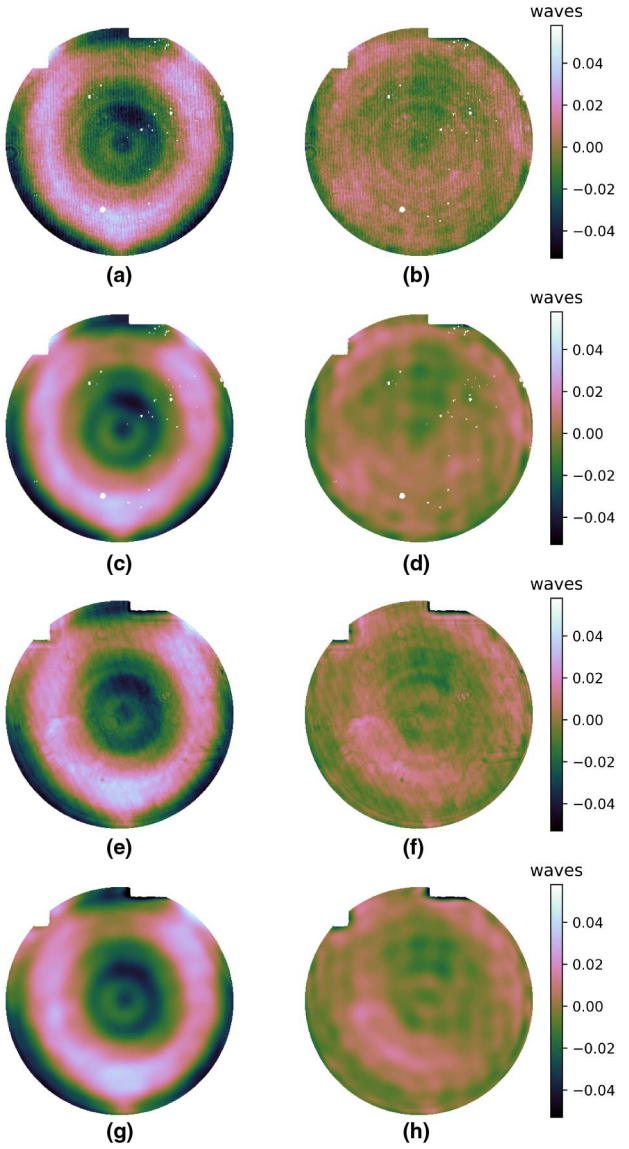

Fig. 4. Comparison of TTDPR with interferometric data. White spots are due to data dropout in the interferogram. (a) Dynafiz high-pass. (b) Difference with TTDPR. (c) Dynafiz band-pass. (d) Difference with TTDPR. (e) Verifire high-pass. (f) Difference with TTDPR. (g) Verifire band-pass. (h) Difference with TTDPR.

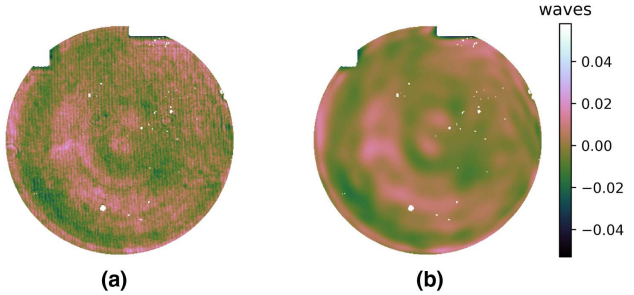

Fig. 5. Computed difference between Dynaphase and Verifire data. (a) High-pass. (b) Band-pass.

Table 1. Summary of Computed Differences between Surface Measurements

	High-Pass	Band-Pass
Dynafiz v. TTDPR	0.0075λ RMS	0.0060λ RMS
Verifire v. TTDPR	0.0072λ RMS	0.0068λ RMS
Dynafiz v. Verifire	0.0073λ RMS	0.0054λ RMS

In summary, we have demonstrated an optical surface measurement in reflection using the TTDPR technique. Using a relatively simple experimental arrangement, we characterized the surface topography of a concave mirror in a tilted configuration. We observed 0.0027λ RMS difference between two TTDPR measurements from separate datasets. Furthermore, we observed good agreement between TTDPR and interferometric measurements of the same mirror from two separate commercial interferometers. This work demonstrates the viability of TTDPR as a relatively inexpensive, yet still accurate, alternative to optical interferometry for full-aperture optical surface characterization.

Funding. National Science Foundation (NSF) (IIP-1338877, IIP-1338898).

REFERENCES

1. M. Guizar-Sicairos and J. R. Fienup, Opt. Express **16**, 7264 (2008).
2. M. Guizar-Sicairos and J. R. Fienup, Opt. Express **17**, 2670 (2009).
3. G. R. Brady, M. Guizar-Sicairos, and J. R. Fienup, Opt. Express **17**, 624 (2009).
4. D. B. Moore and J. R. Fienup, Appl. Opt. **55**, 2526 (2016).
5. D. B. Moore and J. R. Fienup, Appl. Opt. **55**, 4596 (2016).
6. A. M. Michalko and J. R. Fienup, Opt. Lett. **43**, 1331 (2018).
7. J. R. Fienup, Appl. Opt. **21**, 2758 (1982).
8. J. R. Fienup, J. C. Marron, T. J. Schulz, and J. H. Seldin, Appl. Opt. **32**, 1747 (1993).
9. J. R. Fienup, Appl. Opt. **32**, 1737 (1993).
10. J. M. Rodenburg and H. M. L. Faulkner, Appl. Phys. Lett. **85**, 4795 (2004).
11. M. Guizar-Sicairos and J. R. Fienup, Proc. SPIE **7076**, 70760A (2008).
12. T. P. Zielinski and J. R. Fienup, *Frontiers in Optics* (2009), paper SWA2.
13. G. R. Brady and J. R. Fienup, Appl. Opt. **48**, 442 (2009).
14. P. Murphy, G. Forbes, J. Fleig, P. Dumas, and M. Tricard, Opt. Photon. News **14**(5), 38 (2003).
15. D. Malacara, *Optical Shop Testing*, Wiley Series in Pure and Applied Optics (Wiley, 2007).
16. G. R. Brady and J. R. Fienup, Opt. Express **14**, 474 (2006).
17. C. Zhu, R. Byrd, P. Lu, and J. Nocedal, ACM Trans. Math. Softw. **23**, 550 (1997).
18. A. S. Jurling and J. R. Fienup, J. Opt. Soc. Am. A **31**, 1348 (2014).
19. A. M. Michalko and J. R. Fienup, *Optical Design and Fabrication (Freeform, IODC, OFT)* (2017), paper OW2B.5.
20. A. M. Michalko and J. R. Fienup, in *ASPEN/ASPE 2017 Spring Topical Meeting* (2017).
21. B. H. Dean and C. W. Bowers, J. Opt. Soc. Am. A **20**, 1490 (2003).
22. C. J. Evans and R. N. Kestner, Appl. Opt. **35**, 1015 (1996).